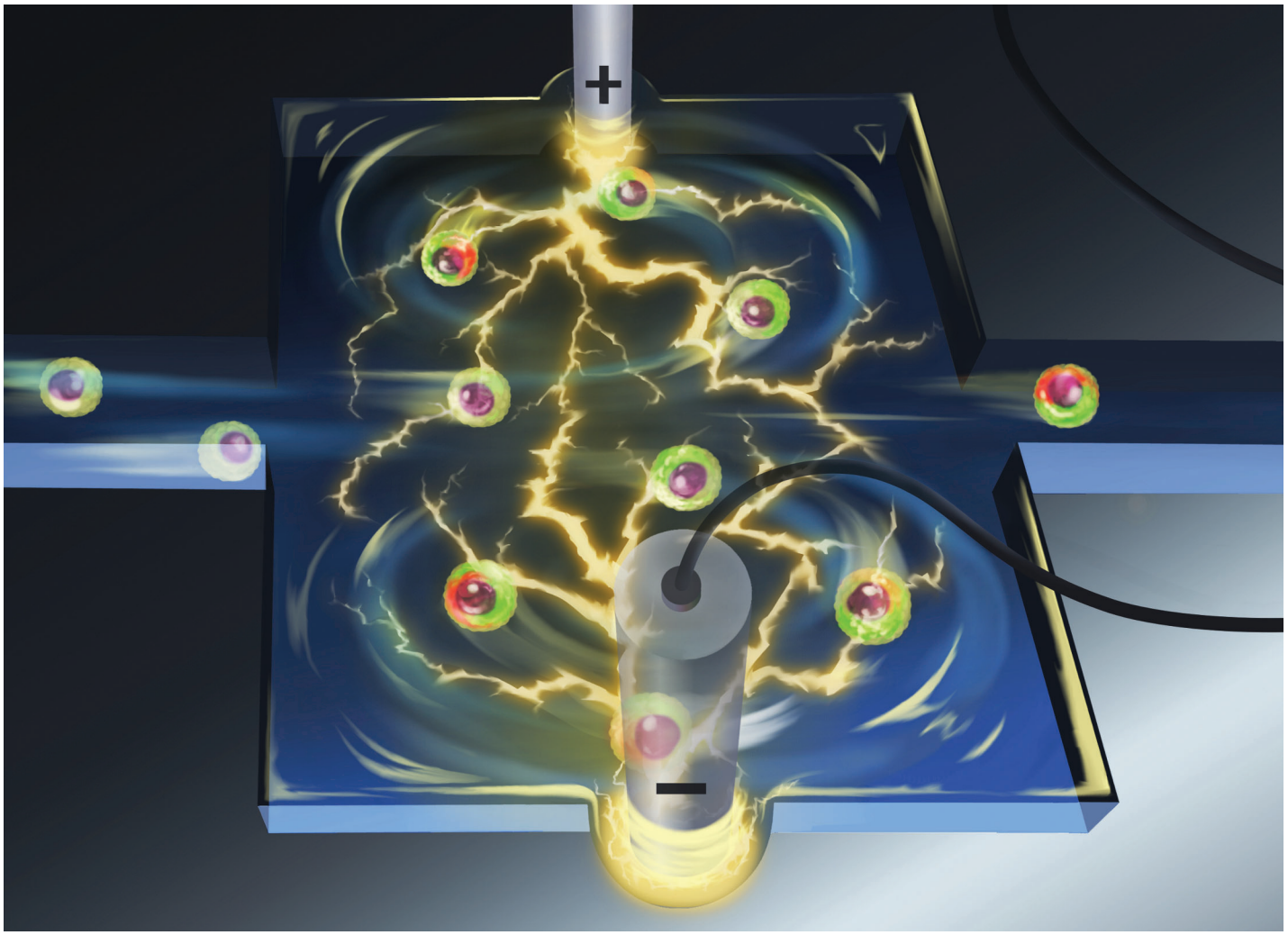

Featuring work from the Microfluidic Biophysics Laboratory of Rowland Junior Fellow Soojung Claire Hur, Rowland Institute at Harvard University, USA.

Title: Sequential multi-molecule delivery using vortex-assisted electroporation

A vortex-assisted microfluidic electroporation system is developed for sequential delivery of multiple molecules into pre-selected target cell populations with precise and independent dosage controllability and improved sample viability.

As featured in:

See Hoyoung Yun and Soojung Claire Hur, *Lab Chip*, 2013, **13**, 2764.

RSC Publishing

www.rsc.org/loc

Registered Charity Number 207890

Lab on a Chip

RSC Publishing

PAPER

Sequential multi-molecule delivery using vortex-assisted electroporation†

Cite this: *Lab Chip*, 2013, **13**, 2764

Hoyoung Yun and Soojung Claire Hur*

Received 12th February 2013,
Accepted 25th April 2013

DOI: 10.1039/c3lc50196e

www.rsc.org/loc

We developed an on-chip microscale electroporation system that enables sequential delivery of multiple molecules with precise and independent dosage controllability into pre-selected identical populations of target cells. The ability to trap cells with uniform size distribution contributed to enhanced molecular delivery efficiency and cell viability. Additionally, the system provides real-time monitoring ability of the entire delivery process, allowing timely and independent modification of cell- and molecule-specific electroporation parameters. The precisely controlled amount of inherently membrane-impermeant molecules was transferred into human cancer cells by varying electric field strengths and molecule injection durations. The proposed microfluidic electroporation system's improved viability and comparable gene transfection efficiency to that of commercial systems suggest that the current system has great potential to expand the research fields that on-chip electroporation techniques can be used in.

Introduction

The ability to introduce foreign molecules into living cells and human tissues has significant implications for various applications in biological research and medicine. Numerous methods, including virus-mediated, chemical, physical, and optical approaches have been developed in order to deliver exogenous molecules into the cells.[1–5] Currently, a virus-mediated approach is the most efficient way of gene delivery and expression; however, besides only being capable of the delivery of nucleic acids, there are considerable risks accompanied with viral delivery systems, including toxicity, chromosomal integration and immunogenicity.[6,7] Viral approaches are, hence, less than ideal for many clinical and research applications, which require minimal post transplantation risks, such as gene therapies and studies of cellular reprogramming or lineage conversions.[8–12]

Consequently, non-viral molecular delivery techniques have begun to gain more attention as inevitable alternatives.[13–15] Among these techniques, electroporation is considered as an effective and powerful technique because of its ability to introduce countless types of molecules into target cells both *in vitro* and *in vivo* without the need for potentially cell-damaging chemical reagents or viruses. Electroporation utilizes short high-voltage pulses to transiently and reversibly create pores on a cell membrane, through which molecular probes of interest can be delivered into the cytosol. However, conventional electroporation techniques using cuvettes or microcapillaries rely on a bulk stochastic molecule delivery processes, making those systems ill-suited for applications requiring precise and individually controlled transferred molecular doses.[16,17] Moreover, it is difficult to obtain practical efficiency and viability for samples with large heterogeneity in cell diameter since the electric field strength required to transiently disrupt cellular membrane is strongly correlated with cell size.[2,18] Therefore, a series of optimization processes, considering numerous performance-determining factors, should be conducted to achieve a high permeabilization efficiency with minimal cell death. Recent advances in microfluidics facilitated the development of microscale electroporation techniques, allowing single-cell level electroporation and dosage control of transferred molecules with enhanced cell viability.[16,19–25] Despite their noteworthy improvement in throughput and molecular delivery efficiency with enhanced viability, a single-directional flow-through scheme, under which most of the current microfluidic electroporation systems operate, renders current microfluidic electroporators inapplicable for emerging research and pharmaceutical applications requiring multi-molecular delivery with an independently controlled amount. Indeed, there are rapidly increasing demands for multi-gene and/or multi-molecular delivery systems for cellular reprogramming studies, development of multigenic disorder therapy, as well as production of industrial and pharmaceutical compounds.[10,26–30]

In this study, we have developed a microfluidic vortex-assisted electroporation system, allowing the sequential and independently tunable delivery of multiple molecules into pre-selected identical populations of target cells. A size-based pre-

The Rowland Institute at Harvard University, 100 Edwin H. Land Boulevard, Cambridge, MA 02142, USA. E-mail: hur@rowland.harvard.edu; Fax: +1 617 497 4627; Tel: +1 617 497 4713

† Electronic supplementary information (ESI) available: Movie 1; Fig. 1–8. See DOI: 10.1039/c3lc50196e

purification step incorporated in the system yielded a uniform size and number distribution, thus, contributed to enhancing the delivery efficiency and viability. The amount of inherently membrane-impermeant molecules transferred into cancer cell lines could be independently controlled through timely modification of electroporation parameters with the aid of real-time process monitoring. The optimum conditions for individual cellular and molecular types were determined by quantitatively examining changes in electroporation efficiency and viability corresponding to systematically varied electrical parameters. Finally, metastatic breast cancer cells were co-transfected with green and red fluorescent protein-expressing plasmids and the results were compared with conventional cuvette test outcomes. The system's high sample viability and electroporation efficiency coupled with minimized sample-loss and sequential multi-molecule delivery capability suggest that the current system has great potential to expand research fields where on-chip electroporation techniques can be applicable.

Materials and methods

Cell preparation

Both adhering (metastatic breast cancer cell line, MDA-MB-231) and suspending (leukemia cell line, K562) mammalian cell lines were cultured in the growth media suggested by American Type Culture Collection (ATCC). The growth media of MDA-MB-231 cells consists of Leibovitz's L-15 medium (Cellgro®, Mediatech, Inc., USA) supplemented with 10% (v/v) fetal bovine serum (FBS, Gibco®, Life technologies, USA) and 1% penicillin–streptomycin (Sigma-Aldrich Co., USA), while that of K562 cells consists of Iscove's Modified Dulbecco's Medium (IMDM, Lonza Ltd., Swiss) supplemented with 10% (v/v) fetal bovine serum, 0.5% gentamicin sulfate (Sigma-Aldrich Co., USA), and 1% penicillin–streptomycin. MDA-MB-231 and K562 cells were cultured in a humidified incubator at 37 °C with 0 and 5% CO_2 environments, respectively. Cells were harvested for experiments 2 days after seeding. The harvested cells were resuspended in Dulbecco's phosphate buffered saline (DPBS, 1×, without Ca^{2+} and Mg^{2+}, Cellgro®, Mediatech, Inc., USA) to have a final concentration ranging from 1×10^5 to 1×10^6 cells ml^{-1}. A Scepter 2.0 (Millipore, USA) was used to determine the cell concentration.

Device design and working principle for target cell pre-isolation and electroporation

A subpopulation of cells were pre-isolated from a heterogeneous population utilizing the previously reported microscale cell trapping mechanism.[31,32] The vortex-assisted trapping allowed maintaining selected cells within the electroporation chambers throughout the entire course of electroporation processes and releasing them off-chip after the process was completed. We have used identical cell trapping chamber dimensions to that of the previously reported device[31] with an auxiliary modification for the electrode embedment (see ESI† Fig. 1). In brief, the microfluidic device consists of an inlet with multiple injection ports and coarse filters, a straight rectangular inertial focusing channel (L = 4.5 cm, W = 40 μm, and H = 60 μm), electroporation chambers (W_c = 400 μm) with two embedded platinum electrodes (d = 500 μm and L_e = 1 mm), and an outlet. Each injection port is assigned for solutions independently containing (i) biological samples to be electroporated, (ii) biomolecules to be delivered to electroporated biological samples, and (iii) the cell growth media or DPBS that flushes the entire device in-between steps, and in which processed cells are resuspended post-electroporation.

The casting mold was fabricated by a photolithography technique using a negative photoresist (KMPR 1050, Microchem, USA) on a 4 inch silicon wafer. The thickness of a developed photoresist was measured using a surface profiler (Dektak 6M, Veeco, USA). The microfluidic patterns were transferred from the mold to polydimethylsiloxane (PDMS, Dow corning, USA) by a conventional casting method. PDMS was degassed and cured overnight in an oven maintained at 70 °C. The cured PDMS sheet with microchannel patterns was delaminated from the mold and punched to create through holes for the inlets, outlet and electrode insertions. Finally, the PDMS sheet and a glass slide were treated with the oxygen plasma cleaner (Technics Micro-RIE, USA) in order to create enclosed microfluidic channels.

When heterogeneous cell populations are injected into the device, cells can be inertially focused to distinct lateral equilibrium positions near the channel walls depending on their biophysical properties (*e.g.*, size and deformability).[31,33,34] Previous work reported that this particle/cell ordering phenomenon could result from a balance between two counteracting inertial lift forces, namely a wall effect lift and a shear-gradient lift, acting on flowing cells (see ESI† Fig. 1a). As inertially focused flowing cells enter the suddenly-expanding electroporation chamber region, the shear-gradient lift alone induces lateral migration of flowing cells towards the core of microscale vortex, since the magnitude of the wall effect lift that had entrained cells at the distinct lateral positions in the straight focusing channel diminishes due to disappearance of channel walls from the vicinity of flowing cells. Since the shear-gradient lift force scales with the third-power of the cell's diameter,[35] larger cells are prone to migrate much more rapidly toward the vortex core than smaller cells are. Once larger cells migrate close enough to vortices, they remain trapped in the vortices while smaller cells were being flushed out of the device. This gentle and stable cell trapping mechanism allows cascading additional biological assays *in situ*. The sample injection time was varied from 20 to 30 s at the fixed operating pressure of 40 psi in order to investigate time-dependent variations in the size and number of trapped cells in the electroporation chambers.

Rapid exchange of multiple solutions

The rapid exchange of multiple solutions was enabled using a custom-built, computer-assisted pneumatic flow control system that timely and independently pressurizes individual solution chambers to drive flow through the microfluidic electroporator. The design was inspired from the automated valve controller developed by Rafael Gómex-Sjöberg, Ph.D., and the list of commercially available flow power components

and polyurethane tubes was obtained from the LBNL Microfluidics Lab's webpage (http://microfluidics.lbl.gov/valve-controllers). The design is modified with add-on features to meet the requirements of the current system (see ESI† Fig. 2). The pneumatic flow control system consists of (i) a compressed nitrogen gas cylinder (Airgas®, USA), (ii) two pressure regulators (a high-pressure regulator (Airgas®, USA) and a downstream regulator (McMaster-Carr®, USA)), (iii) a high-speed 3/2 way-8 valve manifold (Festo, USA), (iv) an in-house built disposable vial holder and (v) inline check valves (IDEX Health and Science, USA). Polyurethane tubes (Pneumadyne, USA) were used to deliver a gas stream through the 8-valve manifold, whereas PEEK tubings (IDEX Health and Science, USA) were used to inject solutions through the current microfluidic system. A disposable sample vial holder was designed such that conventional 50 mL conical bottom centrifuge tubes can be tightly secured in a vertical orientation. Four leak-resistant 50 mL centrifuge tube caps were press-fitted into the machined anodized-aluminum vial holder so that centrifuge tubes could be easily discarded after use. PEEK tubings were securely connected at the inlet and outlet of disposable solution vials using PEEK tubing adaptors (IDEX Health and Science, USA) mounted on the vial holder. It enabled the convenient routine cleaning of used PEEK tubings as they could be easily disassembled from and reassembled into adaptors with a simple twist of threaded ports. Check vales were installed at each PEEK tubing immediately before the microfluidic device's inlet ports in order to ensure one directional flow, preventing cross-contamination of solutions throughout the entire course of the experiments.

A custom-designed electronic controller was also built to rapidly switch the high-speed eight 3/2-way valves (only 4 were used in the current study). The valve controller is composed of the open source microcontroller platform, Arduino uno (www.ni.com/arduino). The firmware for the Arduino is LVIFA, written by Sam Kristoff, and Kevin Fort at National Instruments. Labview-based software communicates *via* USB to the microcontroller to drive individual valves, and the digital input/output of the Arduino drives a pair of Darlington transistor arrays, Allegro Micro ULN2003AN.

The performance of rapid solution exchange by the pneumatic flow control system was verified by measuring time-dependent fluorescent intensity variation across the electroporation chambers during solution exchange between a pure and 1 μM FITC-containing DPBS (see ESI† Fig. 3).

Electrical equipment for electroporation

The electrical equipment for generating high-voltage short-pulses in the electroporation chambers consists of a pulse generator (HP, USA), a high voltage amplifier (Trek Inc., USA), and two platinum electrodes. The electrodes were directly in contact with a solution in the electroporation chambers *via* additional ports placed 1 mm apart, L_e (see ESI† Fig. 1a). The magnitude of applied square wave pulses, V, was varied from 10 to 200 V to have the electric field strength, $E = V L_e^{-1}$, applied across the electroporation chambers ranging from 0.1 to 2 kV cm^{-1}. The magnitude and duration of applied pulses were varied simultaneously in order to determine the optimum electrical condition for sequential multi-molecule delivery. Applied electrical parameters were monitored in real time using an oscilloscope (Agilent, USA). The electric field distribution across the cell-trapping microscale vortices in the electroporation chambers was numerically simulated using COMSOL Multiphysics® (v4.0, Comsol group, USA) in order to investigate whether trapped cells would exposed to a uniform electric field during the electroporation step (see ESI† Fig. 4).

Vortex-assisted electroporation for sequential molecule delivery

Four injection ports were used for the dual molecular delivery test and were individually assigned for a cell sample, a washing solution (DPBS), and two molecular solutions (see Fig. 1a). Each solution was injected into the device sequentially at the operating pressure of 40 psi (equivalent to the flow rate of 400 μL min^{-1}) using the custom-designed pneumatic flow control system. Prior to the cell solution injection, the washing solution was injected for >1 min in order to prime the flow speed required for stable microscale vortex generation. Then, target cells are isolated into the electroporation chambers using the microvortex trapping mechanism simply by switching the active solution port from the washing solution to the cell solution. Once the desired size and number distribution of trapped cells has been achieved, solution is rapidly exchanged to the washing solution in order to remove non-trapped contaminating cells from the entire device without disturbing the orbits that the trapped cells created. After the device is flushed for 20 s, solutions containing the first and the second molecule to be transferred (*e.g.*, fluorescent nucleic dyes or fluorescent protein plasmids) were sequentially injected. Single or multiple short pulses of high electric field were applied promptly after the injection of each molecular solution had been initiated. Magnitude, duration and number of square pulses, as well as incubation time, could be individually varied depending on cellular and molecular types to have better experimental outcomes. Upon completion of molecular delivery using electroporation, the processed cells were resuspended in the washing solution and released from the device for downstream analysis by simply lowering the operating pressure to below 5 psi, followed by a final device flushing step at 40 psi for 10 s.

Fluorescent molecules used for device optimization

Two nucleic acid fluorescent dyes (Propidium iodide (PI) and YOYO®-1, Life Technology, USA) were used to access the current system's electroporation efficiency. The choice of the fluorescent dye combination was made because of their membrane-impermeablility for living cells and negligible emission spectra overlap (maximum emission wavelength: PI, 617 nm and YOYO®-1, 509 nm). Their intrinsic characteristics provide important empirical means to semi-quantitatively determine penetration success rates for each molecule. The final concentration of PI and YOYO®-1 diluted in DPBS was 15 μM and 1 μM, respectively.

In order to identify viable cells pre- and post-electroporation, various fluorescent live-cell staining dyes (2 μM Calcein Blue AM, 2 μM Calcein Green AM and NucBlue®, Life technology, USA) were selectively used depending on the emission spectra of delivered molecules. Co-localization of

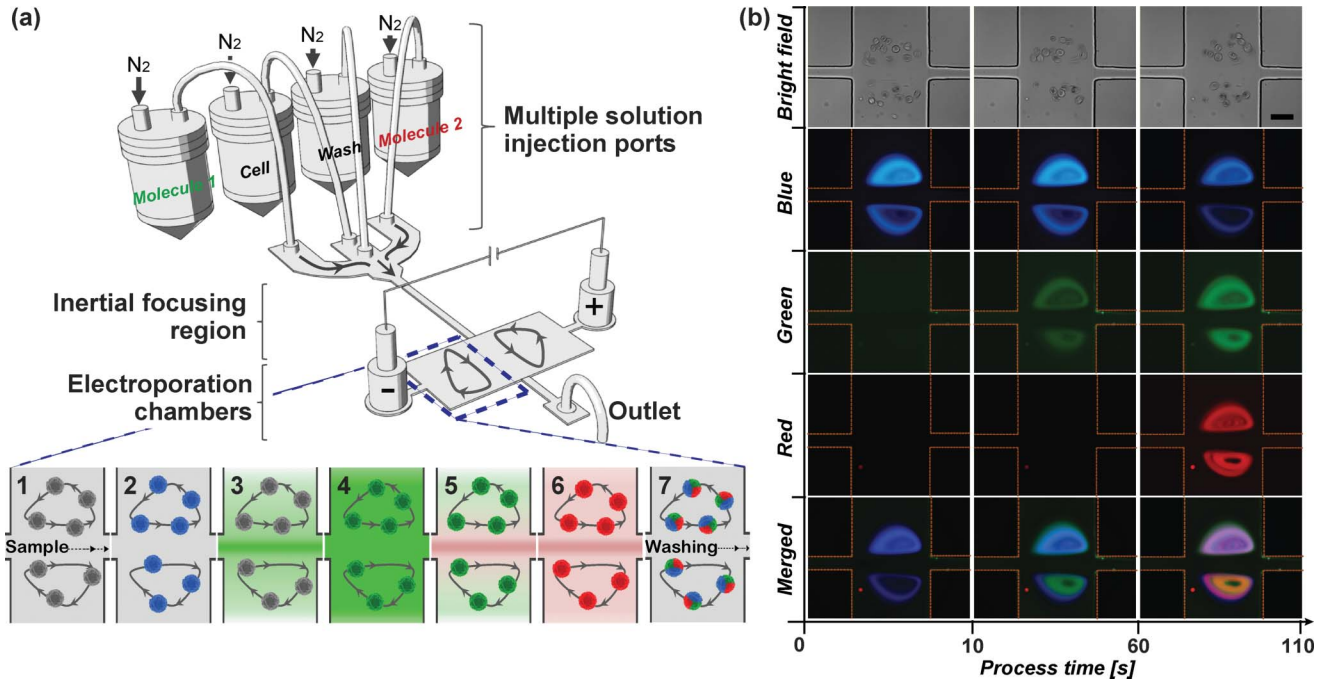

Fig. 1 (a) A schematic representation and (b) fluorescent and bright-field microscopic images illustrating the sequential multi-molecule delivery using the current microfluidic electroporation system. The system consists of the pressure-driven solution injection ports, the inertial focusing region, the electroporation chambers, and the outlet. Each injection port is assigned to the cell sample, a washing solution, and two solutions individually containing transferred molecules. MBA-MD-231 cells, pre-stained with live-cell dye (Calcein AM blue), are isolated and maintained in the electroporation chambers using the microvortices, and the device is flushed with a washing solution to remove contaminating small cells (step 1–2, $t < 10$ s). Promptly after the high-voltage short pulsation ($E = 0.8$ kV cm^{-1}, $t_w = 20$ ms), electroporated cells were incubated for a sufficient time in individual molecular solutions to sequentially deliver two inherently membrane-impermeable molecules (PI at step 3–4, $10 < t < 60$ s and YOYO®-1 at step 5–6, $60 < t < 110$ s). Electric pulses were applied shortly before each molecular delivery step. Image contrast has been enhanced by adjusting the look-up table (LUT). Scale bar is 100 μm.

fluorescent signals from delivered molecules and a live-cell staining dye indicated that the uptake of the tested molecules is solely through electroporation. The viability of processed cells was assessed by staining electroporated cells both on-chip and off-chip. For the on-chip viability test, a solution containing 2 μM Calcein Green AM was injected for 5 min into the device shortly after a washing step post electroporation. For experiments requiring off-chip staining, processed cells were incubated in 2 μM Calcein Green AM solution for 5 min. For gene transfection efficiency tests, cells were stained with NucBlue™ and 0.4% trypan blue (Cellgro®, Mediatech, Inc., USA) to distinguish viable cells from dead cells.

Preparation of fluorescent protein plasmids

Two reporter genes, modified enhanced green fluorescent protein plasmids (pQCXIP-NLS-Vx3-mEGFP, Addgene plasmid 35529,[36] denoted mEGFP hereafter) and modified red fluorescence protein plasmids (pcDNA3-mRFP, Addgene plasmid 13032, denoted mRFP hereafter) were used to determine the transfection efficiency of the current system. Reporter genes were purchased from Addgene in the form of stab cultures of *E. coli* transformed with each gene and plasmids were recovered from *E. coli* cultures by following Addgene's suggested protocol. A Qiagen Plasmid Maxi Kit (Qiagen, USA) was used to extract and purify the plasmids from transformed *E. coli* liquid cultures by following the manufacturer's protocol. The concentration and purity of extracted plasmids were determined by measuring the absorbance at 260 nm and the ratio of absorbance at 260 nm and 280 nm, respectively, using Nanodrop 2000 (Thermo Fisher Scientific Inc., USA). The size and quality of extracted plasmids were verified using electrophoresis on E-gel® 0.8% agarose (E-gel® iBase™ Power System and Safe Imager™ Real-Time Transilluminator, Invitrogen, USA). Moreover, MDA-MB-231 cells were chemically transfected using Lipofectaimine® LTX with Plus™ (Invitrogen) by following the manufacturer's protocol in order to confirm that fluorescent proteins would be expressed upon successful transfection of tested plasmids (see ESI† Fig. 5). Both mEGFP and mRFP were individually diluted in DPBS to have a final concentration of 15 μg ml^{-1}.

Conventional cuvette electroporation test

Transfection efficiency of a conventional electroporation technique is tested in parallel using the BTX electroporation system with 2-mm gap cuvettes with parallel-plate aluminum electrodes (BTX Technologies Inc., USA). Electrical parameters equivalent to those used for the current microfluidic device were applied to the conventional electroporation system using a square-pulse high-voltage pulse generator with a 10 A capability.

High-speed and fluorescent microscopic imaging

High-speed microscopic images of pre-isolated, orbiting target cells were obtained using an inverted microscope (Eclipse Ti, Nikon, Japan) equipped with 150 W Xenon light source (Oriel® Instruments, USA) and a high speed CMOS camera (The Phantom® v1210, Vision Research Inc., USA). 1280 × 400 pixel images were acquired at 4000 frames s^{-1} with an exposure time of 3 μs. Fluorescent microscopic images were acquired using an inverted microscope equipped with a mercury light source (Intensilight, Nikon, Japan), fluorescent filter cube sets, and a CCD camera (Clara, Andor, USA). ImageJ software was used for post image analysis.

Results and discussion

Pre-isolation of cells with uniform size and number distribution

The current system allows achieving uniform size and number distribution of cells trapped in the electroporation chambers with an aid of the microvortex-assisted cell trapping mechanism (see ESI† Fig. 1b). The average size and size-uniformity of the captured cells in the electroporation chambers increased with increasing cell solution injection time. While the average diameter of trapped cells, D_{ave}, was measured to be 20 μm with a coefficient of variation (CV) of 40% shortly after the cell solution injection has been initiated (t = 10 s), the D_{ave} increased to 32 μm with a reduced CV of 25% at t = 30 s. The average number of cells processed in each run was found to be 20 when the maximum size and uniformity have been achieved, and the number of cells was maintained identical throughout the course of the entire electroporation processes.

The ability to trap cells with a uniform size distribution would positively contribute to having better molecular delivery efficiency and cell viability because the cell size distribution has significant implications for membrane permeabilization. When cells are exposed to an extracellular electric field, E, transmembrane potential, $\Delta V_m = fED\cos\theta$, is induced in a cell.[2,37,38] Here, f is the weighting factor, which is the measure of how cells contribute to the applied electric field distribution, and D and θ are the cell diameter and the polar angle measured with respect to the external field, respectively. In order to transiently permeate cells without cell lysis, ΔV_m should exceed the transmembrane potential, ΔV_s, but remain below the irreversible electroporation threshold, ΔV_c. For mammalian cells, ΔV_s is reported to range between 200 mV and 1 V, depending on pulse duration,[39–41] while ΔV_c is expected to be greater than 1 V.[42,43] Previous electroporation tests performed with cell lines that have a large size variation are reported to have low electroporation efficiencies and viabilities[2] since samples with higher size heterogeneity are expected to have a greater number of cells having induced ΔV_m that falls outside of the optimum range for successful transient permeabilization. Therefore, the current system's ability to pre-isolate cells with a higher homogeneity in size would minimize undesirable consequences associated with a large variation in cell size.

Real-time monitoring of sequential multi-molecule delivery

Two membrane-impermeable molecules (PI and YOYO®-1) were sequentially delivered into pre-isolated MDA-MB-231 cells (see ESI† Movie 1 and Fig. 1b). Cells were stained with Calcein AM blue prior to injection in order to ensure that delivery of those membrane-impermeable molecules is solely through transient pores formed by electroporation. Promptly after a short pulsation (E = 0.8 kV cm^{-1} and t_w = 20 ms), the first (YOYO®-1, 10 < t < 60 s) and second (PI, 60 < t < 110 s) molecules were sequentially injected and fluorescent signals, corresponding to each molecule, were observed from electroporated orbiting cells, indicating successful molecular delivery. Uncompromised Calcein AM blue fluorescent intensity post the sequential delivery steps suggests preserved membrane-integrity of processed cells as irreversibly permeated cells with disrupted cell membrane were expected to leach Calcein AM molecules, thus, exhibiting substantial reduction in blue fluorescent intensity. Moreover, real-time monitoring of the entire molecular delivery process permitted determination of cell- and molecule-specific parameters, such as ΔV_s, ΔV_c and the molecular amount for delivery initiation, based on direct observation of cellular responses. Real-time monitoring eliminated the need for numerous independent tests of samples with varying molecular concentration combinations to identify optimum conditions, often required by conventional cuvette electroporation methods. In addition, the current system can be easily scaled to accommodate more types of molecules simply by incorporating a greater number of inlet ports. These results show that the developed system allows independent, quantitative controllability of multi-molecule delivery without the need for time-consuming and labor-intensive sample preparation steps.

Transferred molecular dosage controllability

The proposed system enables precise control of the molecular amount transferred into the pre-selected target cells by varying either electrical field strength or molecular injection time (see Fig. 2). The amount of transferred PI molecule proportionally increased with the electric field strength when cells were exposed to the identical molecular amount (*i.e.*, PI solution was injected into the device for 40 s (6.4 μg) and processed cells were washed with molecule-free DPBS for 10 s). It was found that E_i = 0.4 kV cm^{-1} is required to initiate the delivery of PI molecules to the MDA-MB-231 and E exceeding 2.0 kV cm^{-1} resulted in cell lysis. Similarly, the molecular transfer dosage can be monotonically increased by increasing solution injection time with a set electric field strength, E_o = 0.8 kV cm^{-1}. E_o is one of the optimal conditions, where processed cells exhibited high viability (83%) and electroporation efficiency (70%). Electroporated cells' molecular uptake was initiated after cells were exposed to approximately 800 ng of PI (equivalent to the solution injection time, t = 5 s). Experiments conducted for K562 cells exhibited a similar trend to that from the MDA-MB-231 experiments, while a slightly higher E_i = 0.6 kV cm^{-1} and E_o = 1.0 kV cm^{-1} were required (see ESI† Fig. 6). The higher E_i of K562 cells can be attributed to differences in membrane properties or a difference in average diameter between K562 (D_{ave} = 12 μm) and MDA-MB-231 cells (D_{ave} = 15

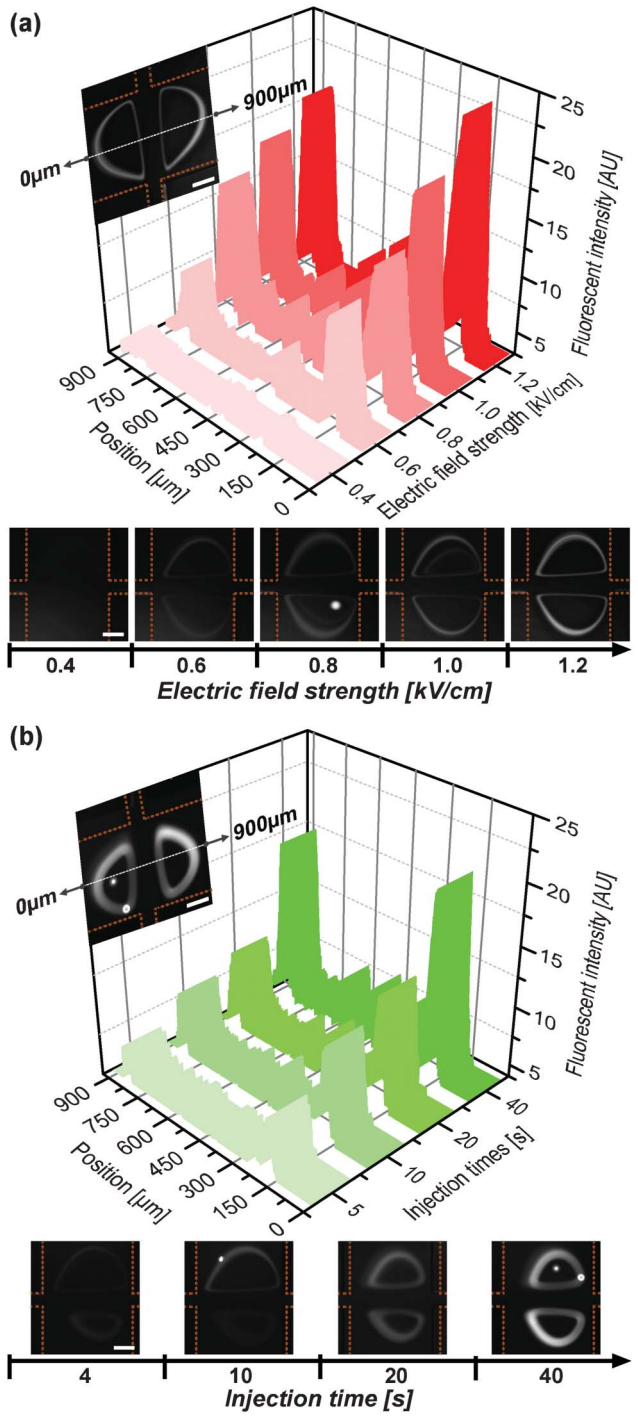

Fig. 2 The proposed system can control the transferred amount of molecules by systematically varying electric field strength and solution injection time. The amount of transferred PI molecules into MDA-MB-231 cells increased with increasing (a) electric field strength with fixed solution-injection and incubation time (40 s) and (b) increasing solution injection time at E = 0.8 kV cm^{-1}. All data were obtained from independently conducted experiments and their fluorescent intensities were quantified using ImageJ software. LUT was adjusted to enhance the contrast. Scale bars are 100 μm.

μm). The system's rapid solution exchange scheme combined with the real-time monitoring ability enabled precise and independent control and optimization of each transferred molecular dosage simply by varying incubating-duration and/or electric field strength.

Optimum electrical parameters for high viability and electroporation efficiency

A series of electroporation experiments with systematically varied electrical parameters were conducted in order to determine the optimum condition for MDA-MB-231 cells. Fig. 3a shows that electroporation efficiency inversely correlates with viability in agreement with previous reports.[2] Cells exposed to E = 0.4 kV cm^{-1} exhibited a viability and electroporation efficiency of 94% and 25%, respectively, whereas those electroporated at E = 1.2 kV cm^{-1} showed a viability and electroporation efficiency of 58% and 92%, respectively. The optimum electric field strengths required to electroporate MDA-MB-231 cells with desirable viability (greater than 83%) and efficiency (greater than 70%) values were found to be in the range between 0.6 and 1.0 kV cm^{-1}.

Interestingly, molecules taken up by cells electroporated using the proposed vortex-assisted system were distributed uniformly across the entire cytosol, while cells electroporated in the identical device under static conditions were partially occupied by delivered molecules (see Fig. 3b and ESI† Fig. 7). Presumably, the gentle and continuous agitation of cells trapped in vortices during the electroporation process that the current system uniquely provides would promote uniform permeabilization, known to be a key factor for improving electroporation efficiency.[25] In fact, cells electroporated using the current system exhibited a 3-fold higher electroporation efficiency than that of previous studies.[2,17,44]

Sequential gene transfection test

As a proof of concept, taking advantage of the superior viability and electroporation efficiency of the proposed system, we conducted multi-gene transfection of MDA-MB-231 cells and the results were compared to those obtained from a conventional cuvette system under the identical electroporation condition (E = 0.7 kV cm^{-1}, t_w = 30 ms and plasmid concentration of 15 μg ml^{-1}). The tested electroporation conditions fell within the range that was previously reported for successful transfection of MDA-MB-231 cells using conventional cuvette systems.[45,46] The transfection efficiency of the proposed system for mEGFP, mRFP and the co-transfection efficiency of both genes were measured to be 6.2%, 9.3% and 3.7%, respectively (see Fig. 4). A substantial reduction in transfection efficiency compared to the previously discussed electroporation efficiency could reflect the expected intracellular degradation and/or insufficient nuclear targeting of delivered plasmids after successful penetration across the cell membrane,[47] and may not necessarily mean a discouraging outcome. The fact that transfection efficiencies of the proposed system were not significantly different from that of the conventional cuvette system ($p > 0.1$) supports the conclusion that the reduction in transfection efficiency is presumably caused by difficulties associated with naked plasmid delivery processes and/or potentially reflects the upper limit for tested plasmids used in electroporation (see ESI† Fig. 8). Enhanced transfection efficiency would be anticipated if plasmids were coated with an intracellular

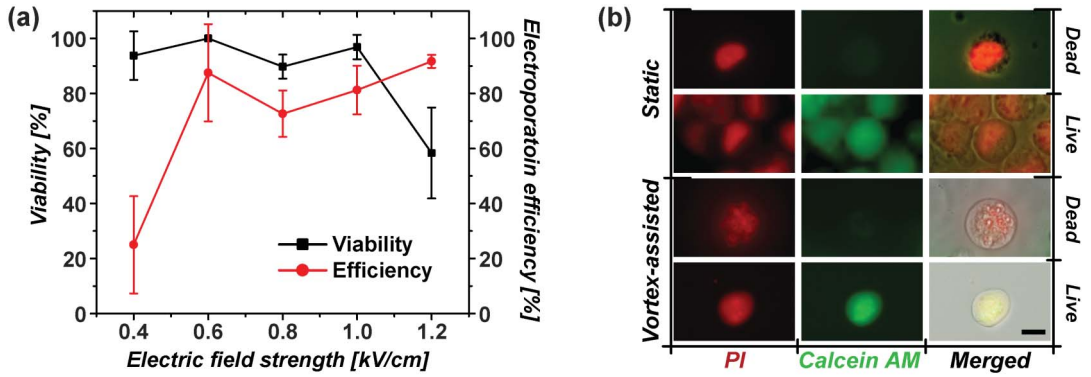

Fig. 3 Viability and electroporation efficiency of MDA-MB-231 cells as a function of the applied electric field strength (n = 4). (a) Viability and electroporation efficiency were inversely correlated with each other. The optimum electric field strength for MDA-MB-231 was found to range between 0.6 and 1.0 kV cm^{-1} with viability and electroporation efficiency greater than 83% and 70%, respectively. (b) Fluorescent images of living and dead cells that were electroporated using the microfluidic system under the vortex-assisted and the static condition. Intracellular molecular distribution was found to be more uniform for continuously orbiting cells during the electroporation process than those processed under the static condition. Scale bar is 10 μm.

degradation preventive layer or conjugated with nuclear-targeting peptide scaffolds.[48–50]

The current system's unique features differentiate it from conventional electroporation methods and grant it the ability to provide transfected cells with higher viability. For instance, the proposed system allows immediate on-chip washing after electroporation, eliminating the adverse effect of residual plasmids on sample viability.[51] Moreover, the system's exceptionally low operational electric current resulted in a temperature rise of less than 1 °C, whereas the instant temperature rise of the conventional cuvette test was calculated to be ΔT = 38 °C from Joule heating when an identical operational electrical field was applied (V = 160 V, L_e = 2 mm and I = 5 A). As anticipated, cells electroporated using the proposed system showed a 7-fold higher viability than that observed from cells processed using the conventional cuvette system (Fig. 4c). Due to the low throughput of the current system (~20 cells/run), the number of viable, co-transfected cells from the conventional system and the proposed technique cannot be directly compared. However, given that the current system transfects cells with a similar efficiency yet superior viability for all tested plasmids, at least a 3-fold increase in number of successfully co-transfected cells is expected from the current system if an identical number of cells is processed. Although the current system's throughput is considerably lower than conventional electroporation systems, the channel geometry is simple and the process can be fully automated. Therefore, the throughput can be improved simply by parallelizing electroporation chambers, as we have demonstrated previously,[31] and electrodes. Furthermore, owing to the simplicity of the solution exchange scheme, the system can be automated to repeatedly process a greater number of cells in a shorter period of time in order to expand its use for more practical applications, requiring the ability to process a larger volume of samples with minimal user interventions.

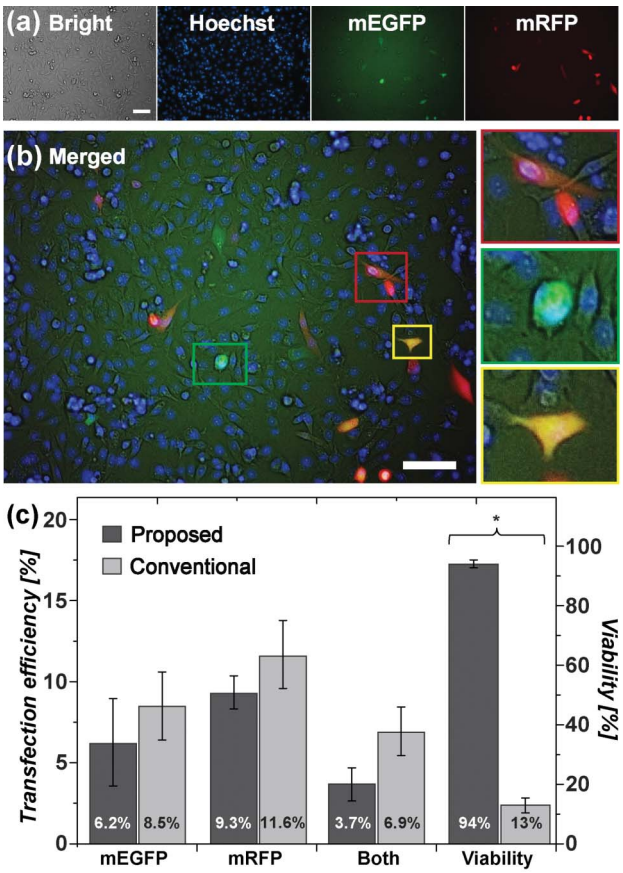

Fig. 4 (a and b) Representative microscopic images of MDA-MB-231 cells obtained 72 h after mEGFP and mRFP co-transfection (E = 0.7 kV cm^{-1} and t_w = 30 ms). Red, green and yellow boxes in the merged image and enlarged views (right) indicate cells transfected with mRFP-only, mEGFP-only, and both genes, respectively. Living cells' nuclei were stained with Hoechst 33345. (c) A comparison of transfection efficiency and viability for the proposed system and the conventional cuvette system (n = 4). The number fraction of transfected cells was similar for all tested plasmids regardless of the system used for electroporation ($P > 0.1$), whereas cells processed using the proposed system exhibited a 7-fold higher viability. Asterisk indicates $P < 0.05$. Image contrast is enhanced by adjusting LUT. Scale bar is 100 μm.

Conclusion

The proposed technique allows on-chip multi-molecular probe delivery without the need for additional target-cell purification and sample preparation in pre- or post-electroporation steps (*i.e.*, laborious sample preparation or time-consuming centrifugation). The transferred molecular amount can be precisely and individually controlled by varying electric field strengths and molecular injection durations. The system's real-time monitoring capability allows timely fine-tuning and modification of individual parameters. Independently controllable electrical parameters based on the molecular probes to be delivered would enable sequential cytosolic delivery of virtually any combination of a broad range of macromolecules with various electrical charges or diffusivity. The system is also applicable to notorious hard-to-transfect suspension cell lines. Moreover, the system's low operational current can eliminate viability-related problems associated with a high current in electroporation. Processed cells using the proposed system exhibited a 7-fold higher viability than the conventional systems; thus, at least a 3-fold higher number of transfected cells was anticipated to be obtained from the current system than its counterparts if the identical numbers of cells were to be processed in both systems. The developed technique has great potential to expedite the development of the multi-gene or multi-molecule transfer process, requiring precise controllability of dosage and electroporation parameters.

Acknowledgements

This work is supported by the Rowland Junior Fellow program. The authors thank scientists and staff at the Rowland Institute at Harvard: Chris Stokes for his help on development of the custom-built, computer-assisted pressure control setup, Diane Schaak, Ph.D. for her informative assistance in gene and cell preparation, Winfield Hill for invaluable guidance for development of the electrical setup, Scott Bevis, Kenny Spencer and Don Rogers for machining mechanical and plumbing components required for the pressure setup and Linda Turner Stern, Professor Howard Berg and Joel Parks, Ph.D. for advice on setting up the high intensity Xenon light source required for high speed microscopic images. Masters for microfluidic devices were fabricated at the Center for Nanoscale Systems (CNS) at Harvard University. We also thank Marc Lim for the artwork.

Notes and references

1 N. Somia, L. Wang and F. Gage, *Genes Resist. Dis.*, 2000, 147.
2 J. Gehl, *Acta Physiol. Scand.*, 2003, **177**, 437–447.
3 D. J. Stevenson, F. J. Gunn-Moore, P. Campbell and K. Dholakia, *J. R. Soc. Interface*, 2010, **7**, 863–871.
4 C. W. Pouton and L. W. Seymour, *Adv. Drug Delivery Rev.*, 1998, **34**, 3–19.
5 A. Sharei, J. Zoldan, A. Adamo, W. Y. Sim, N. Cho, E. Jackson, S. Mao, S. Schneider, M. J. Han and A. Lytton-Jean, *Proc. Natl. Acad. Sci. U. S. A.*, 2013, **110**(6), 2082–2087.
6 S. Hacein-Bey-Abina, A. Garrigue, G. P. Wang, J. Soulier, A. Lim, E. Morillon, E. Clappier, L. Caccavelli, E. Delabesse and K. Beldjord, *J. Clin. Invest.*, 2008, **118**, 3132.
7 Y. Yang, F. A. Nunes, K. Berencsi, E. E. Furth, E. Gönczöl and J. M. Wilson, *Proc. Natl. Acad. Sci. U. S. A.*, 1994, **91**, 4407–4411.
8 F. Jia, K. D. Wilson, N. Sun, D. M. Gupta, M. Huang, Z. Li, N. J. Panetta, Z. Y. Chen, R. C. Robbins and M. A. Kay, *Nat. Methods*, 2010, **7**, 197–199.
9 C. E. Dunbar, *Annu. Rev. Med.*, 1996, **47**, 11.
10 J. B. Kim, B. Greber, M. J. Araúzo-Bravo, J. Meyer, K. I. Park, H. Zaehres and H. R. Schöler, *Nature*, 2009, **461**, 649–643.
11 J. Verhaagen, *Prog. Brain Res.*, 2009, **175**, 151.
12 M. Costa, M. Dottori, K. Sourris, P. Jamshidi, T. Hatzistavrou, R. Davis, L. Azzola, S. Jackson, S. M. Lim and M. Pera, *Nat. Protoc.*, 2007, **2**, 792–796.
13 M. Stadtfeld, M. Nagaya, J. Utikal, G. Weir and K. Hochedlinger, *Science*, 2008, **322**, 945–949.
14 K. Okita, M. Nakagawa, H. Hyenjong, T. Ichisaka and S. Yamanaka, *Science*, 2008, **322**, 949–953.
15 J. Wells, L. Li, A. Sen, G. Jahreis and S. Hui, *Gene Ther.*, 2000, **7**, 541.
16 P. E. Boukany, A. Morss, W.-c. Liao, B. Henslee, H. Jung, X. Zhang, B. Yu, X. Wang, Y. Wu, L. Li, K. Gao, X. Hu, X. Zhao, O. Hemminger, W. Lu, G. P. Lafyatis and L. J. Lee, *Nat. Nanotechnol.*, 2011, **6**, 747–754.
17 W. G. Lee, U. Demirci and A. Khademhosseini, *Integr. Biol.*, 2009, **1**, 242–251.
18 A. Agarwal, I. Zudans, E. A. Weber, J. Olofsson, O. Orwar and S. G. Weber, *Anal. Chem.*, 2007, **79**, 3589–3596.
19 W. G. Lee, H. Bang, H. Yun, J. Min, C. Chung, J. K. Chang and D. C. Han, *Lab Chip*, 2008, **8**, 224–226.
20 J. A. Kim, K. Cho, Y. S. Shin, N. Jung, C. Chung and J. K. Chang, *Biosens. Bioelectron.*, 2007, **22**, 3273–3277.
21 T. Geng, Y. Zhan, J. Wang and C. Lu, *Nat. Protoc.*, 2011, **6**, 1192–1208.
22 J. Lin, R. Chen, S. Feng, Y. Li, Z. Huang, S. Xie, Y. Yu, M. Cheng and H. Zeng, *Biosens. Bioelectron.*, 2009, **25**, 388–394.
23 J. Olofsson, K. Nolkrantz, F. Ryttsén, B. A. Lambie, S. G. Weber and O. Orwar, *Curr. Opin. Biotechnol.*, 2003, **14**, 29–34.
24 M. Wang, O. Orwar, J. Olofsson and S. G. Weber, *Anal. Bioanal. Chem.*, 2010, **397**, 3235–3248.
25 J. Wang, Y. Zhan, V. M. Ugaz and C. Lu, *Lab Chip*, 2010, **10**, 2057–2061.
26 M. Buntru, S. Gärtner, L. Staib, F. Kreuzaler and N. Schlaich, *Transgenic Res.*, 2012, 1–15.
27 S. Ozbas-Turan, C. Aral, L. Kabasakal, M. Keyer-Uysal and J. Akbuga, *J. Pharm. Pharm. Sci.*, 2003, **6**, 27–32.
28 D. W. Han, N. Tapia, A. Hermann, K. Hemmer, S. Höing, M. J. Araúzo-Bravo, H. Zaehres, G. Wu, S. Frank and S. Moritz, *Cell Stem Cell*, 2012, **10**(4), 465–472.
29 H. J. Cho, C. S. Lee, Y. W. Kwon, J. S. Paek, S. H. Lee, J. Hur, E. J. Lee, T. Y. Roh, I. S. Chu and S. H. Leem, *Blood*, 2010, **116**, 386–395.
30 K. Okita, T. Ichisaka and S. Yamanaka, *Nature*, 2007, **448**, 313–317.

31 S. C. Hur, A. J. Mach and D. Di Carlo, *Biomicrofluidics*, 2011, **5**, 022206.
32 A. J. Mach, J. H. Kim, A. Arshi, S. C. Hur and D. Di Carlo, *Lab Chip*, 2011, **11**, 2827–2834.
33 S. C. Hur, H. T. K. Tse and D. Di Carlo, *Lab Chip*, 2010, **10**, 274–280.
34 D. Di Carlo, *Lab Chip*, 2009, **9**, 3038–3046.
35 D. Di Carlo, J. F. Edd, K. J. Humphry, H. A. Stone and M. Toner, *Phys. Rev. Lett.*, 2009, **102**, 094503.
36 J. J. Sims, F. Scavone, E. M. Cooper, L. A. Kane, R. J. Youle, J. D. Boeke and R. E. Cohen, *Nat. Methods*, 2012, **9**, 303–309.
37 T. Kotnik, F. Bobanović and D. Miklavčič, *Bioelectrochem. Bioenerg.*, 1997, **43**, 285–291.
38 H.-Y. Wang and C. Lu, *Anal. Chem.*, 2006, **78**, 5158–5164.
39 E. Tekle, R. D. Astumian and P. B. Chock, *Biochem. Biophys. Res. Commun.*, 1990, **172**, 282–287.
40 E. Neumann, S. Kakorin and K. Tœnsing, *Bioelectrochem. Bioenerg.*, 1999, **48**, 3–16.
41 J. F. Edd, L. Horowitz, R. V. Davalos, L. M. Mir and B. Rubinsky, *IEEE Trans. Biomed. Eng.*, 2006, **53**, 1409–1415.
42 R. Davalos, L. Mir and B. Rubinsky, *Ann. Biomed. Eng.*, 2005, **33**, 223–231.
43 B. Rubinsky, *Technol. Cancer Res. Treat.*, 2007, **6**, 255.
44 S. Movahed and D. Li, *Microfluid. Nanofluid.*, 2011, **10**, 703–734.
45 X. Shen and M. Falzon, *Exp. Cell Res.*, 2006, **312**, 3822.
46 T. Tanaka, B. Dancheck, L. Trifiletti, R. Birnkrant, B. Taylor, S. Garfield, U. Thorgeirsson and L. De Luca, *Mol. Cell. Biol.*, 2004, **24**, 3972–3982.
47 D. Luo and W. M. Saltzman, *Nat. Biotechnol.*, 2000, **18**, 33–37.
48 R. J. Lee and L. Huang, *Crit. Rev. Ther. Drug Carrier Syst.*, 1997, **14**, 173.
49 S. Katayose and K. Kataoka, *Bioconjugate Chem.*, 1997, **8**, 702–707.
50 A. Subramanian, P. Ranganathan and S. L. Diamond, *Nat. Biotechnol.*, 1999, **17**, 873–877.
51 T. Geng, Y. Zhan, J. Wang and C. Lu, *Nat. Protoc.*, 2011, **6**, 1192–1208.

Electronic Supplementary Material (ESI) for Lab on a Chip

Electronic Supplementary Information (ESI)

Sequential multi-molecule delivery using vortex-assisted electroporation

Hoyoung Yun and Soojung Claire Hur*
The Rowland Institute at Harvard University, Cambridge MA, USA

*To whom the correspondence should be addressed: hur@rowland.harvard.edu

List of Supplementary Movie

Supplementary Movie 1. Sequential delivery of two inherently membrane impermeable molecules (YOYO®-1 and PI) into metastatic breast cancer cell lines (MDA-MB-231)

List of Supplementary Figures

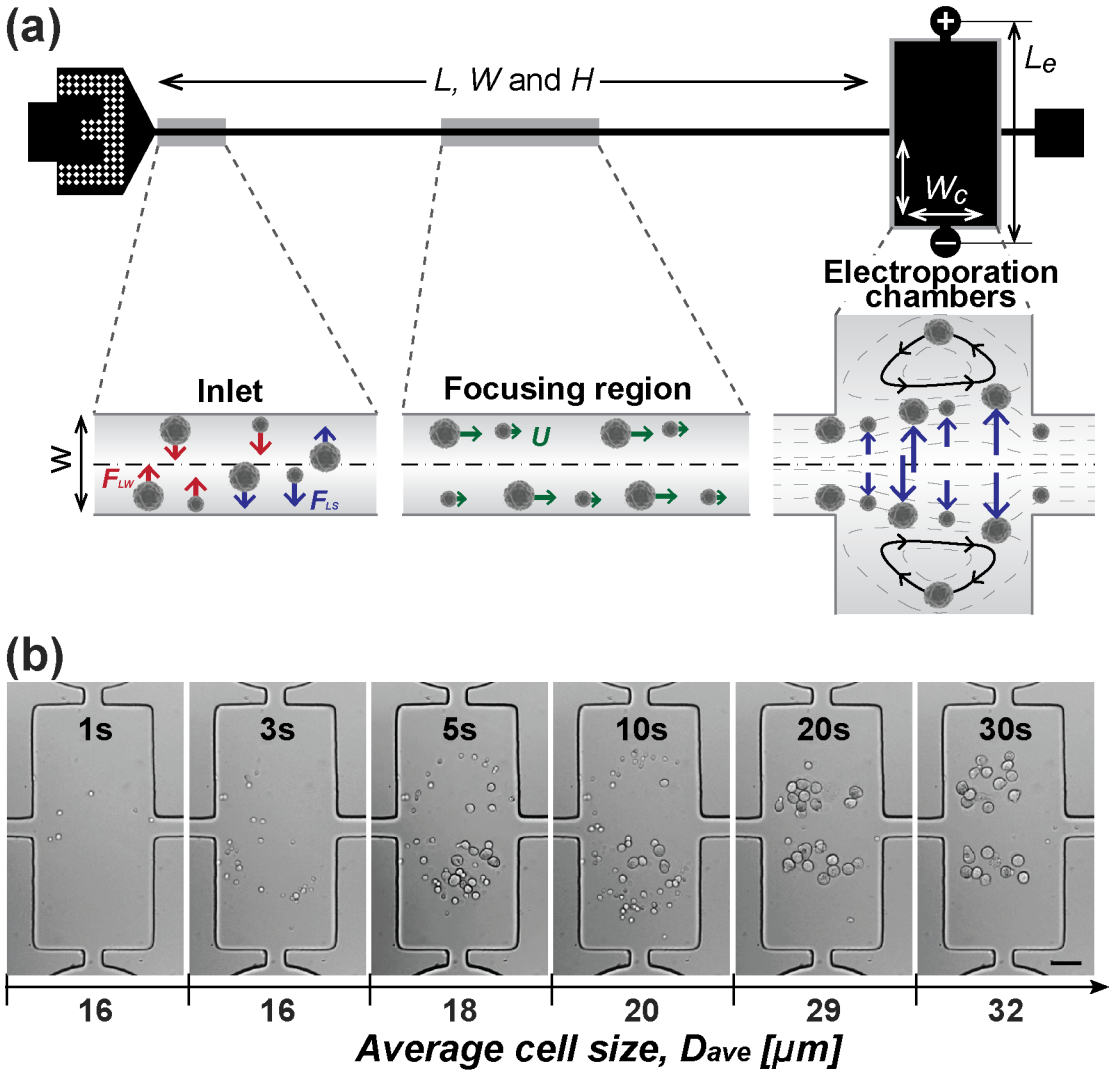

ESI Figure 1. (a) Device design and cell trapping principle. The device consists of the inlet region, the focusing region (L = 4.5 cm, W = 40 μm, and H = 60 μm), the electroporation chambers (W_c = 400 μm and L_e = 1mm), and the outlet. Injected cells experience wall effect lift, F_{LW}, and shear-gradient lift, F_{LS}, in the focusing region, resulting in sized-dependent lateral focusing and traveling velocity, U. When cells enter the electroporation chambers, cells with diameter larger than the threshold (D_t ~ 15 μm) are trapped in microscale vortices while smaller cells are flushed out of the device. (b) Average cell diameter and uniformity in size distribution of the trapped cells increased with the sample injection time. The average diameter of the captured metastatic breast cancer cells increased from 20 ± 8.5 μm (coefficient variation (CV) of 40%) to 32 ± 7.9 μm (CV of 25%) with increasing cell solution injection time. Image contrast is enhanced using ImageJ. Scale bar is 100 μm.

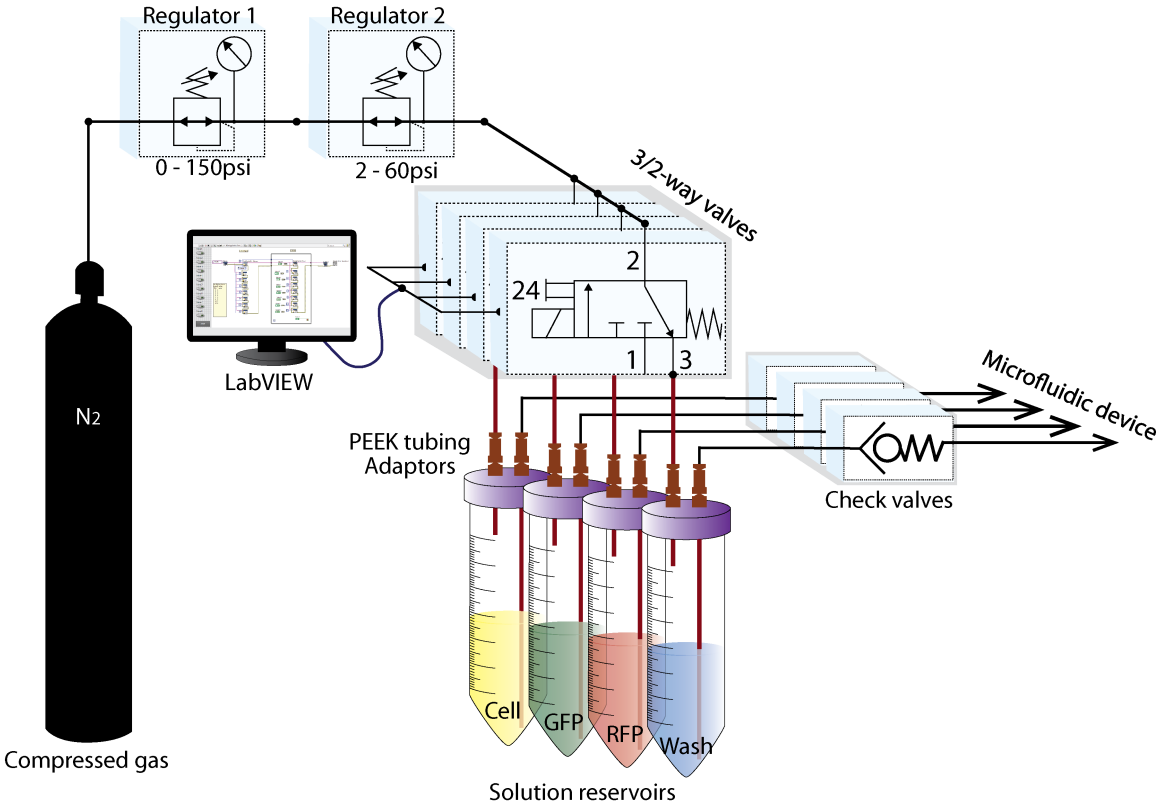

ESI Figure 2. Schematic of the computer-assisted pneumatic flow control system. Standard International Standard Organization (ISO) graphic symbols were used to better convey individual pneumatic components' functionality. Note that diagram is not to scale.

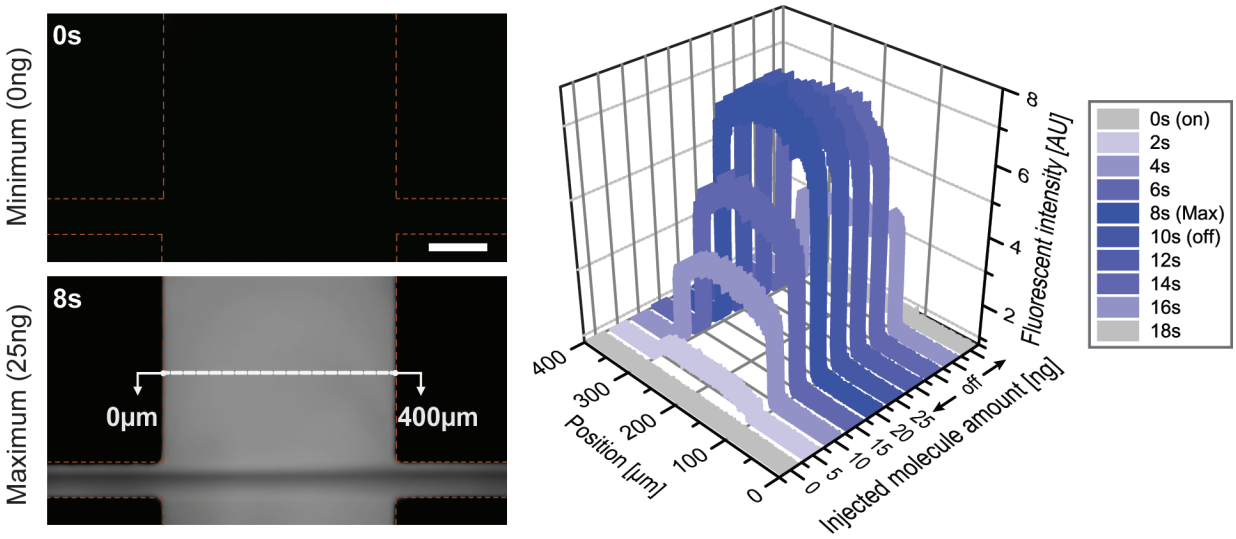

ESI Figure 3. Rapid solution exchange demonstration using a 1 µM FITC solution and a washing solution (DPBS). Time required to saturate the electroporation chambers with the desired molecular solution (t = 8 s) was found to be identical to that required to completely flush those chambers, suggesting a symmetric solution exchange scheme. Total injected amount of FITC molecules was 25 ng when saturation occurred. Image contrast is enhanced by adjusting look-up table (LUT). Scale bar is 100 µm.

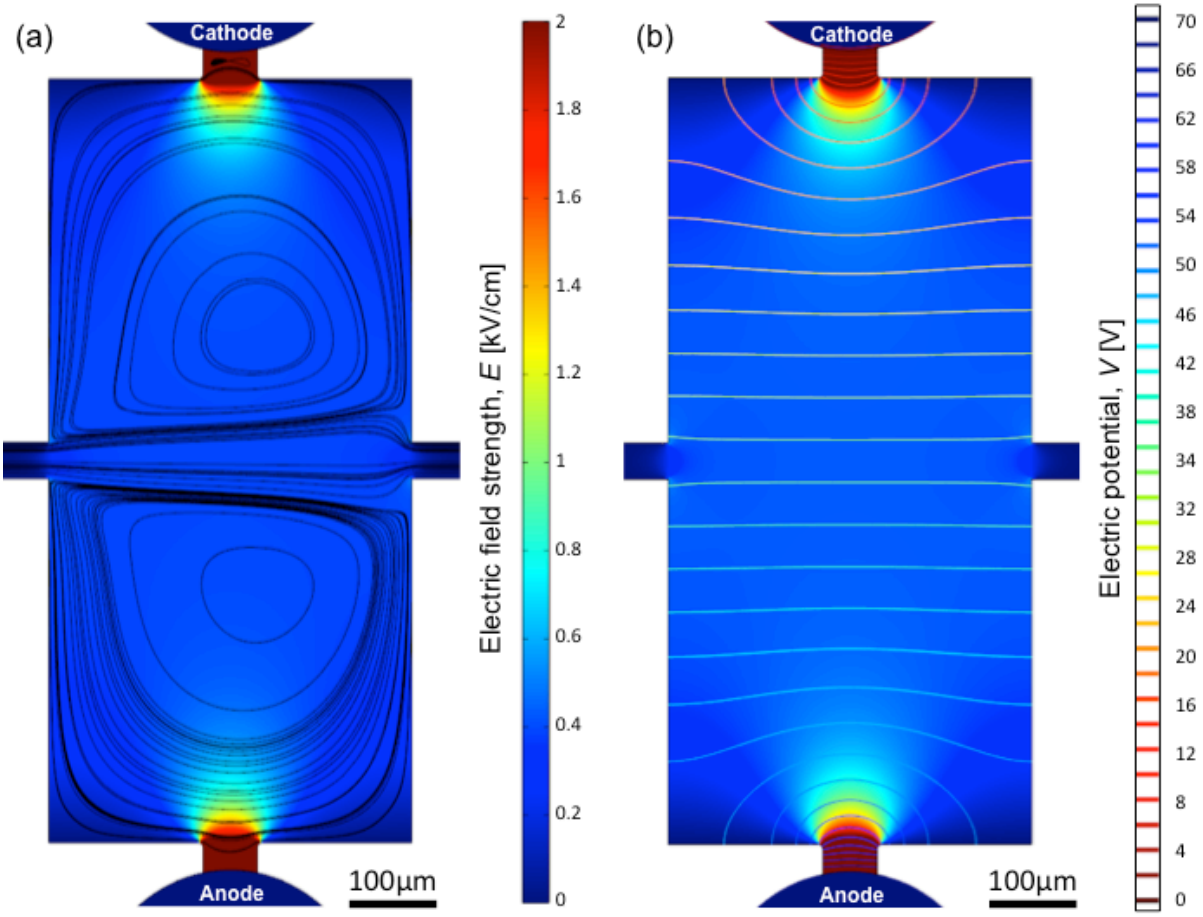

ESI Figure 4. Numerical simulations illustrate that the distribution of electric fields in the electroporation chamber is uniform and cell-trapping microscale vortices do not alter the distribution. Computed electric field strength distribution across the electroporation chamber is overlaid with (a) streamlines and (b) electric potential contours. Large gradient of the electric field was observed outside of orbits occupied by captured cells, thus it would not affect the electroporation performance adversely. Moreover, non-trapped cells would not be electroporated because no electric field gradient was observed in the straight inertial focusing channel. The simulation was conducted for 2D incompressible Navier-Stokes mode combined with the Electrocurrent mode using COMSOL® Multiphysics software (version 4.0). The fluid is considered to have the same properties as DPBS at room temperature (density, dynamic viscosity, and electric conductivity of 1000 kg/m^3, 1.005 mPa·s, and 1.4 S/m, respectively). The pressure drop across the simulated region was set to be 20 psi since the electroporation chamber is located at 1.5 cm downstream from the inlet. No-slip boundary conditions were set on the channel walls and on the interfaces between electrodes and the fluid. Density, relative permittivity, and electric conductivity of platinum electrodes were wet to 21,450 kg/m^3, 7, and 9.43×10^6 S/m, respectively. The applied voltage across the two electrodes was set to 70 V.

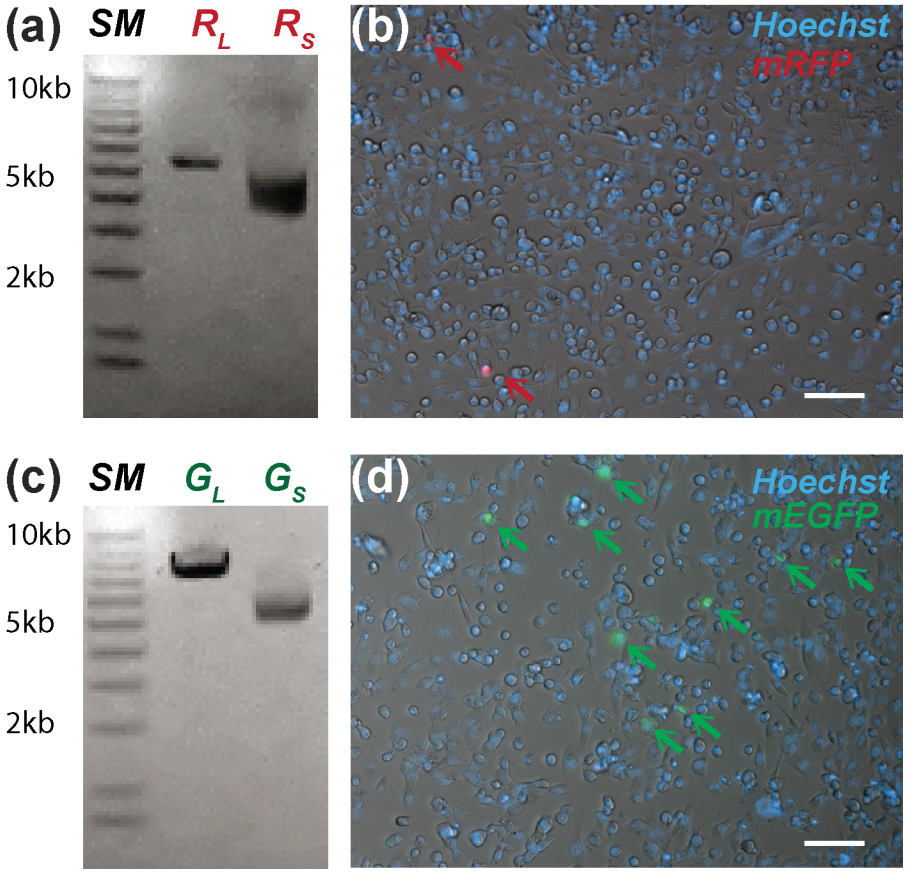

ESI Figure 5. The size and quality of (a and b) pcDNA3-mRFP (6118 bp, denoted as R) and (c and d) pQCXIP-NLS-Vx3-mEGFP (7919 bp, denoted as G) were verified using a gel electrophoresis and a chemical transfection technique. In order to determine the size of entire construction, mRFP and mEGFP plasmids were linearized by selecting BsmI and Nhel-HF enzymes, respectively. Enzymes and reagents were purchased from New England Biolab® Inc. Subscription L and S indicate plasmids existing in full-length linear and supercoiled conformation, respectively. 1 kb DNA ladder (TrackIt™, Invitrogen™ USA) was used as the size marker (SM). Moreover, it was confirmed that MDA-MB-231 cells expressed (b) mRFP and (d) mEGFP once they were chemically transfected with pcDNA3-mRFP and pQCXIP-NLS-Vx3-mEGFP, respectively, using Lipofectaimine® LTX with Plus™ (Invitrogen) by following the protocol suggested by the manufacturer. Red and green arrows indicate cells transfected with mRFP and mEGFP genes, respectively. Transfected living cells were counterstained with Hoechst 33324 (NucBlue® Live ReadyProbes™ Reagent, Life technologies™).

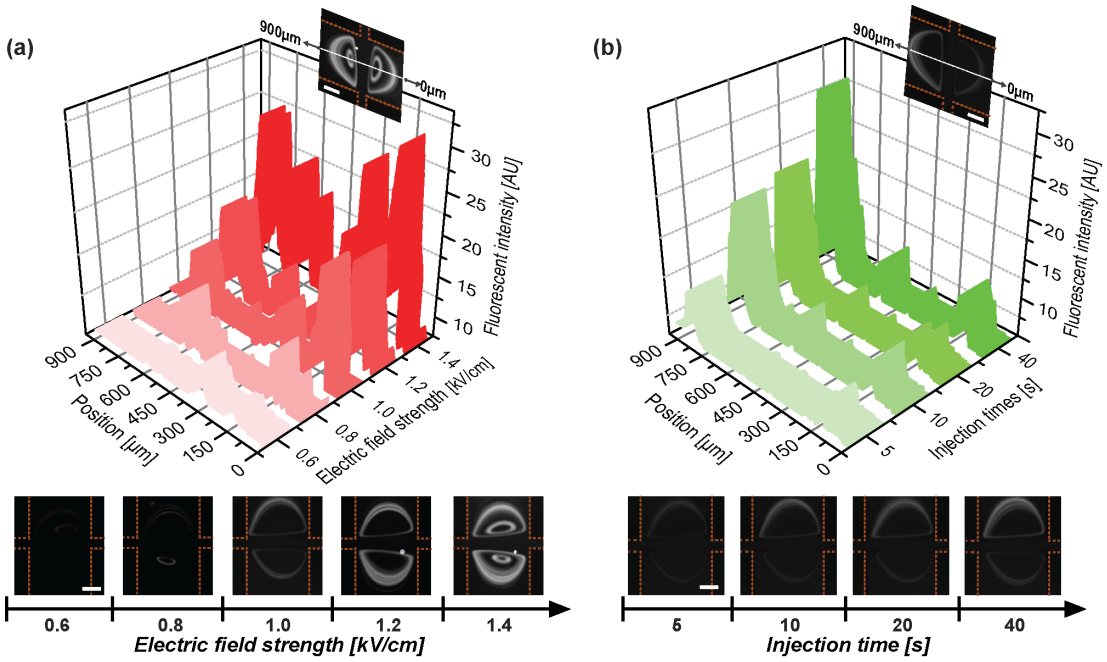

ESI Figure 6. The amount of the transferred PI molecules into K562 cells can be precisely controlled. Similar to MDA-MB-231 results, the amount of transferred PI molecules increased with increasing (a) electric field strength and (b) solution injection time. The electric field strength required to initiate molecular delivery was E = 0.6 kV/cm. All data were obtained from independently conducted experiments and their fluorescent intensities were quantified using the ImageJ software. LUT was adjusted to enhance contrast. Scale bars are 100 μm.

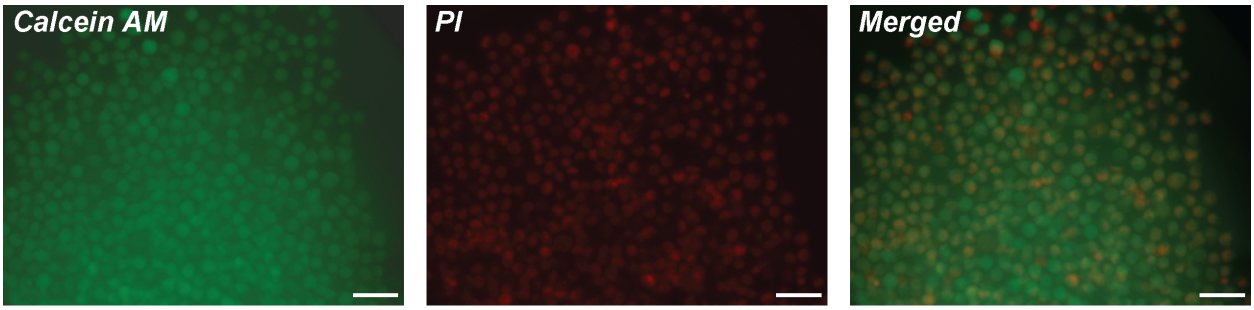

ESI Figure 7. Fluorescent microscopic images of K562 cells electroporated in the identical device under the static condition without vortex-assisted size-based pre-selection (E = 1.5kV/cm). Molecules uptaken by electroporated cells were partially occupied. Living cells were stained with Calcein AM green prior to the electroporation and Propidium iodide (PI) was chosen as a molecule to be delivered. Note that PI uniformly stains non-viable cells, resulting in fluorescent signals overlapping with that of electroporated cells. Scale bars are 100 μm.

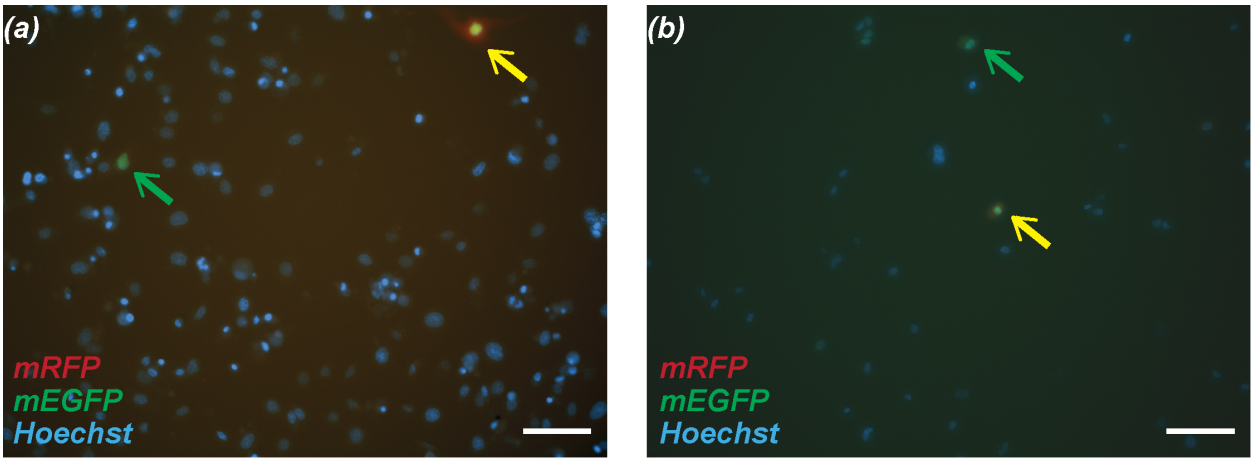

ESI Figure 8. Representative fluorescent microscopic images of MDA-MB-231 cells obtained 48 hours after mEGFP and mRFP co-transfection using the conventional cuvette-type electroporation system at (a) E = 0.4kV/cm and (b) E= 0.8 kV/cm. While the viability of processed cells were strongly affected by increased electric field strength, apparent enhancement in the transfection efficiency has not been observed. Green and yellow arrows indicate cells transfected with mEGFP-only and both mEGFP and mRFP genes, respectively. Nuclei of living cells were stained with Hoeschst 33342 (NucBlue® Live ReadyProbes™ Reagent, Life technologies™).. Scale bars are 100μm.